

ATA Mapping of the Geostationary Belt Toward RFI Excision

G. R. Harp

7/28/09

Abstract

We performed tests to demonstrate ATA capabilities for mapping (more specifically, for determining the positions of) satellites in the Geostationary belt. Observations were made over a period of several hours with static (Az, El) pointings at different positions on the belt, with 60 second integration times at each pointing. The center frequency was 4002 MHz, in the middle of the C-band allocation for TV satellites, which rather thoroughly occupies the frequency range 3.6-4.3 GHz. Calibration is difficult in this frequency range because the satellites overwhelm celestial sources even when pointed far from the GEO belt. Observations at about 100 pointings are mosaicked into a strip spanning 55 degrees in azimuth and 1 degree in elevation, with good qualitative success.

Introduction

Astronomical observations are often corrupted by satellite emissions, perhaps most predictably by Geostationary (GEO) satellites whose sky positions move very slowly and transmissions are foreseeable. While two-line element ephemerides (<http://celestrak.com/>) and public domain integrators are available they may not have sufficient accuracy (few hundred arcsec accuracy at high altitudes, much poorer for low earth orbit satellites) to allow deterministic nulling methods to cancel their contributions to astronomical images. Realistic simulations of deterministic nulling at the ATA350¹ suggest that single-point nulls with suppression levels -50 dB relative to the main beam peak have a width of ~30", almost 100x smaller than the diameter of the synthetic beam. At the Square Kilometer Array (SKA), deterministic nulls will be orders of magnitude smaller. Thus to apply deterministic methods in actual observations it may be necessary to use more accurately determine satellite positions in data reduction.

In this memo we probe the feasibility of using astronomical measurements on GEO satellites to determine their positions. This position info can be fed back into simple deterministic nulling schemes to remove the satellite emissions from astronomical data. While most RFI excision schemes rely on adaptive excision or nulling, adaptive schemes are often more complex and can null only signals that can actually be measured. Deterministic (i.e. direction dependent) nulling has the advantage of simplicity of implementation and can null signals that are below the detection limit of the instrument. But there are practical limits. Experimental studies at the SETI institute show that array calibration errors place substantial limits on null depth, allowing interferers to corrupt astronomical images (P. Backus, et al., private communication). Even so, deterministic nulling has its place in the astronomers toolbox for mitigating RFI.

TV Sat Spectral Occupancy

While pointing ATA at 3c274 (a supernova remnant), frequency spectra were acquired from the correlator. All cross-correlation amplitude spectra were averaged and squared to give power. Integration time is 10s per 100 MHz band, except for the first and last which are 70s (resulting in a change in signal to noise level). The bands were not overlapped, so there are small gaps of unusable data beginning and end of each band (does not influence conclusions).

Figure 1 shows that C-band satellites overwhelm the astronomical signal over 800 MHz, despite strong emission 3c274. Dotted lines show empirical boundaries of the spectral occupancy. Discontinuities are evident every 100 MHz because satellite transmissions are time variable and the data were taken serially. The strongest signals are as large as 4000 in these units (off scale), while the astronomical signal is <10 units.

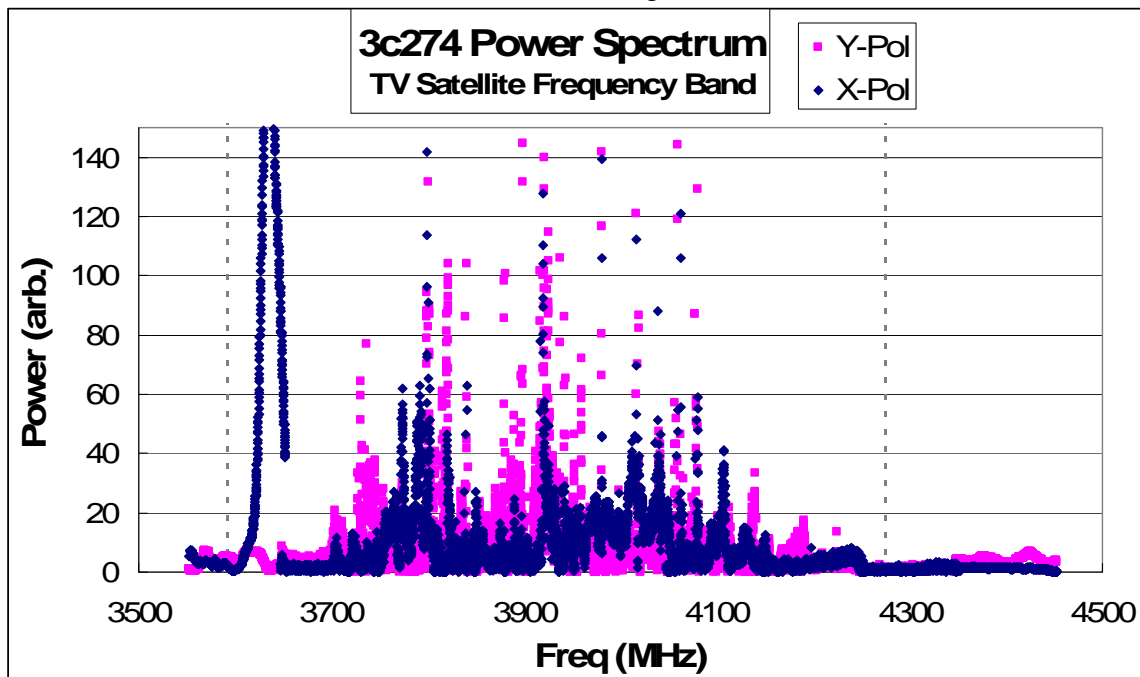


Figure 1: Baseline-averaged cross correlation spectra on the X and Y polarizations of ATA over the frequency range occupied by C-band satellites near 4 GHz. Dotted lines delimit an empirical range where these satellites dominate even the very strong astronomical signal from 3c274 (Virgo A). The two polarizations show drastically different curves, indicating that these satellites have high degrees of linear polarization. In the “clean” regions, amplitude oscillations are visible because these spectra have not been corrected for the spectral bandpass of the instrument.

Calibration

Our goal is to make a mosaicked map of a swath of the geostationary belt in the middle of the occupied band in Fig. 1 (4002 MHz). This is a challenging task because ordinary calibration techniques are not feasible. The usual method of ping-ponging between the target and quasar (point source) calibrator will not work because quasars are many orders of magnitude weaker than the satellite transmissions. Even when pointed away from the geostationary belt, enough stray power from satellites enters the system to confound the

calibration. Other methods of interpolating coherent bandpass phases from one frequency to another are problematic for two reasons – the frequency span is very large (± 400 MHz) and the ATA bandpass function is not well calibrated at the present time.

Instead we use an incoherent approach to bandpass calibration via the image domain. We use the strongest, relatively compact cm-wave continuum source in the sky, CasA, as a calibrator.¹ The signal from CasA gives $>10\times$ signal to interference ratio (SIR) in a few minute observation near 4 GHz. Because CasA is resolved (see below) with ATA42 at 4 GHz we self-calibrate CasA with a previously defined map of its structure.

The input map for CasA calibration can be generated from an established catalog like NVSS. We had some concern that because the baseline distances at ATA are substantially smaller than at VLA, there might be some artifacts introduced when calibrating short baselines. Frankly, it was simply more convenient to generate CasA calibration maps using ATA42 itself, which by definition has the best baseline distribution for calibration. The chicken/egg problem of getting a CasA map at 4002 MHz was solved by obtaining maps from “spectrally clean” regions above and below the desired frequency. Maps were made using uncorrupted channels (see Fig. 1) below 3600 MHz and above 4350 MHz. These two maps are averaged² and displayed in Fig. 2.

¹ Mel Wright points out that the Sun is stronger still. Even the moon might be a good alternative. These sources are essentially circular to within the limits of our resolution and may be good alternatives since the solar/lunar model is easily computed. However, this sun is a bit too strong – we would have to reduce the system gain by at least 20 dB in order to observe it. This might introduce unexpected calibration errors. Both sun and moon are resolved, even on the shortest ATA baselines, which might introduce quantitative errors. Nevertheless, we intend to seriously consider Sun and Moon calibration in future observations.

² Not averaged directly, though. First we generated a clean map from both images. CasA’s emission is known to vary smoothly with frequency, so the clean maps should be frequency independent apart from an overall scaling factor. So we averaged the clean components for each image and also averaged the residuals. The resultant clean components and residuals were then re-combined (miriad restor method) to generate the average image.

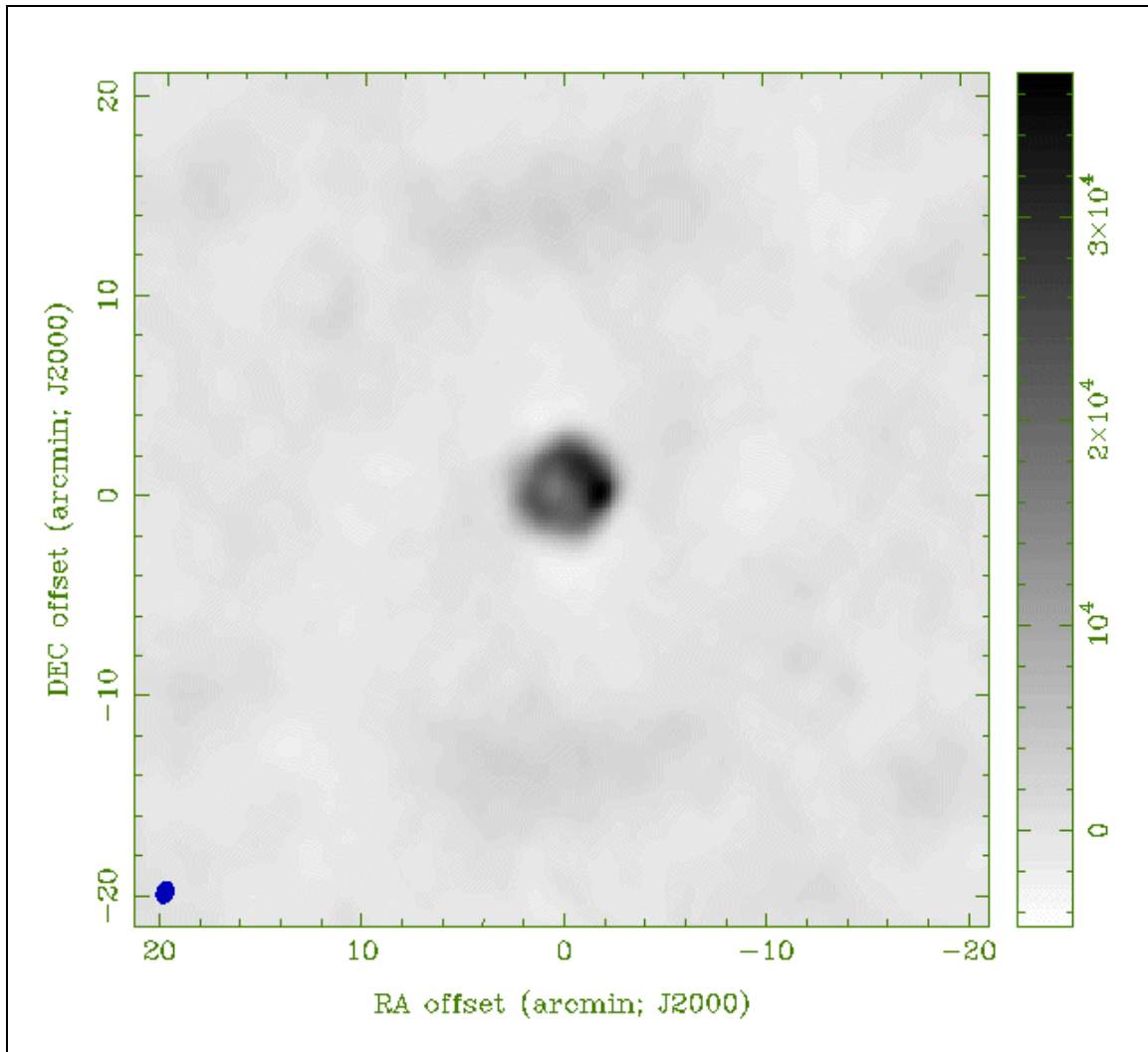


Figure 2: ATA42 map of CasA, averaging maps from 3600 and 4200 MHz.. At each frequency data were acquired in only *four 1-minute observations* over a period of 4.5 hours. This small dataset has a low SIR ~ 15 . Longer duration observations and better RFI excision would do better, but the image is nonetheless interesting as the supernova shell of gas surrounding CasA star is clearly resolved, showing a hot spot on the RHS.

In the next stage, the CasA data acquired at 4002 MHz were self-calibrated using Fig. 2.³ Finally, this phase calibration was transferred to the GEO belt observations were made with ninety 60-second pointings over 4 hours (duty cycle = 37%). The rest of the time was taken up re-pointing the telescopes and in overhead of starting the observing program. This overhead can be reduced substantially when we next attempt such observations.

³ In future studies, we may apply a threshold to Fig. 2 before using it as a reference map, since we know the low-level emission in the image is mostly interference.

A map was generated from each pointing, (invert, clean, restore cycle) and all the maps were mosaicked into one long strip Fig. 3 using the miriad task “linmos.” In fig. 3 one can easily spot 9 satellites transmitting near 4002 MHz. We know these are satellites because their flux is much higher than would be expected for a celestial source. These satellites are concentrated close to the center of the GEO belt as expected.

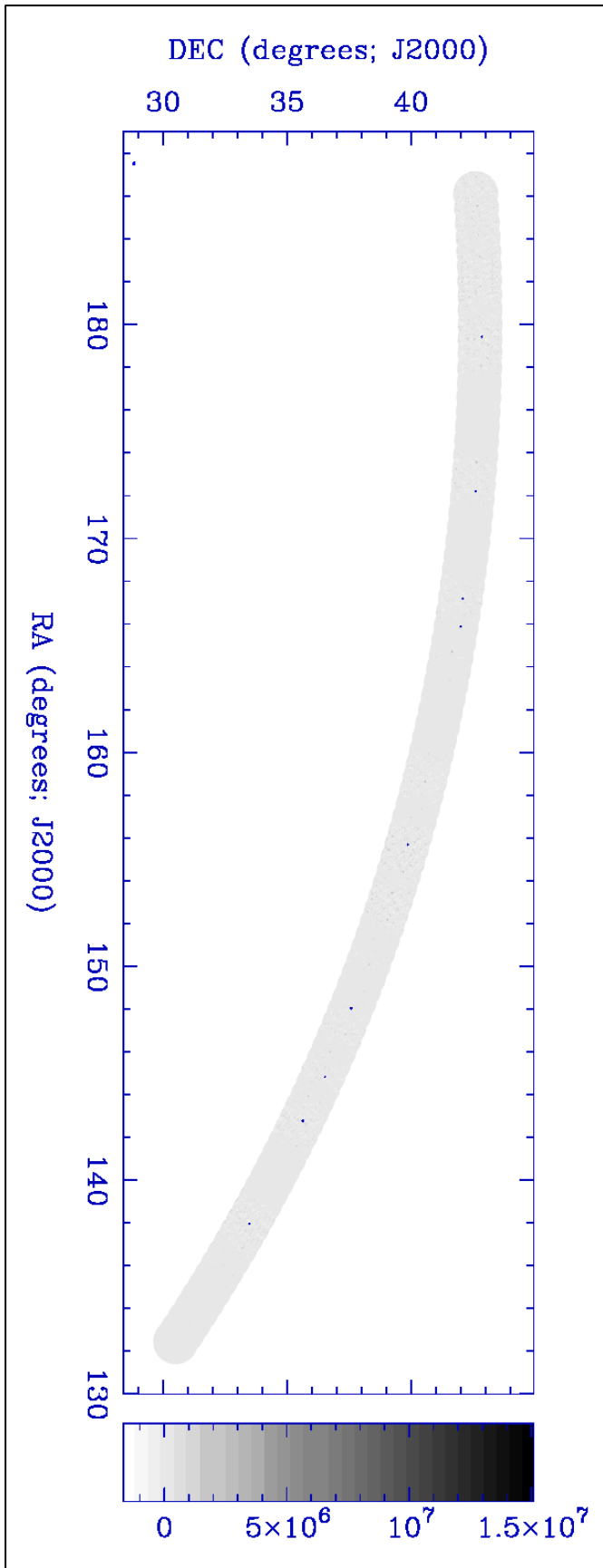


Figure 3: Large scale map of the geosynchronous belt includes a band about 1° wide over a range of azimuthal angle ($188^\circ - 132^\circ$) as seen from HCRO. The map is plotted in both grayscale and with contour lines in yellow. The contours bunch around the position of the satellite giving a small round dot at the positions of strong emitters. Even these tiny dots have been artificially broadened to permit visibility on this scale. The actual size of the satellite dots is $< 1'$, and peak positions may be determined in the arcsec range.

Further detail is revealed in Fig. 4 which blows up a small section of the strip. Because of the greater magnification we can identify more satellites per unit area than in fig. 3. The satellites appear to be resolved (have angular width), however this width is greatly exaggerated by the way we reconstructed the map. All the point sources identified with clean were artificially expanded in size to 10 arcmin by convolution with a Gaussian function. If this were not done, the satellites would hardly be observable on this scale. The same operation was applied to fig. 3. Notice that no smoothing is applied to the residual image which shows fine structure on smaller scales.

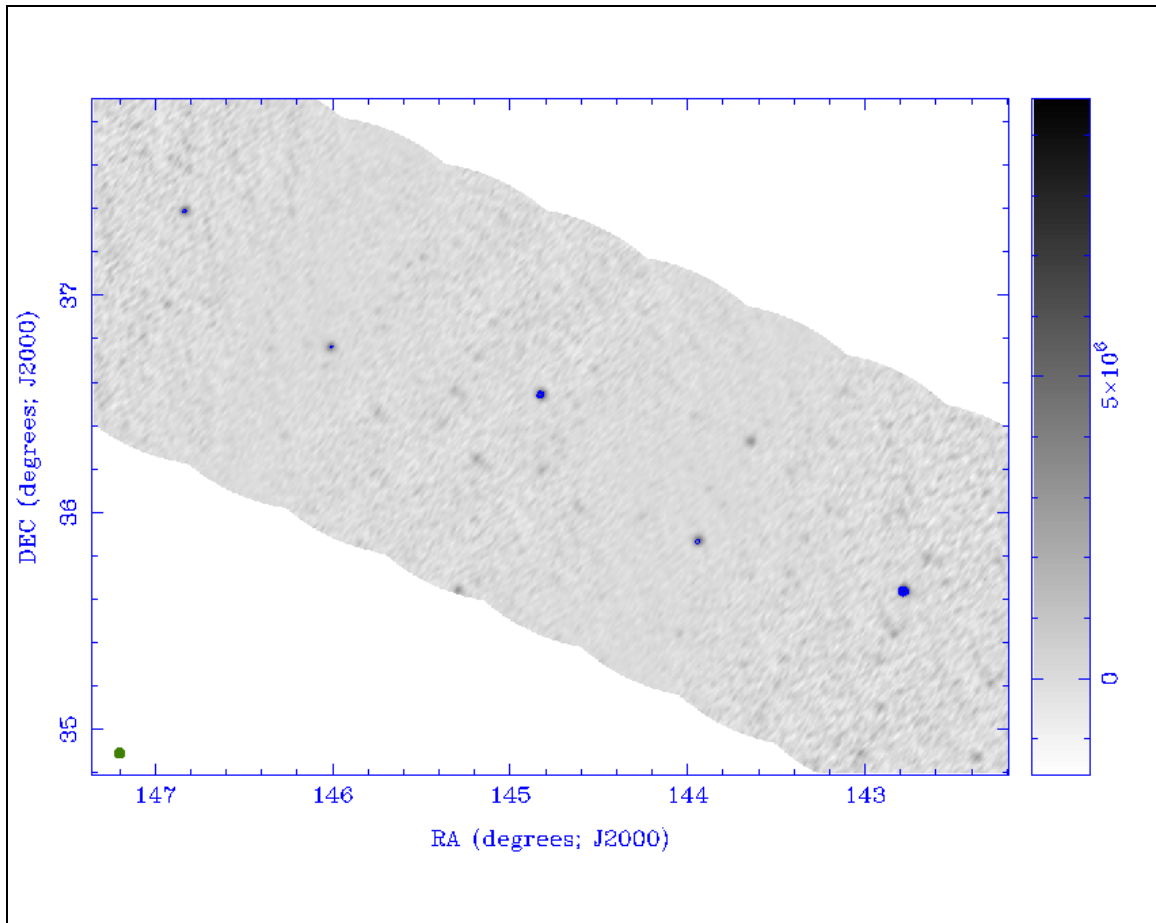


Figure 4: Blow up of a smaller range of azimuth taken from Fig. 3. Note once again that the satellite have been artificially broadened to 10' diameter to enhance visibility. If this were not done, the satellites would occupy less than 1 pixel in the image and be difficult to identify. The residual map has not been smoothed or modified in this way. Figs. 3 and 4 are visual aids to understand the data and not meant to represent the accuracy / SIR present in these images.

Fig. 4 has areas of negative power which is a natural occurrence of the incomplete uv-coverage of our array. In particular, no zero spatial-frequency components are included. Since we expect the satellites to stand out positively, we can achieve greater image contrast by truncating the color scale at zero intensity and plotting negative powers in white. This is done in Fig. 5.

Figure 5 is a blowup of a small region around the brightest satellite in fig. 4. Here we plot the true satellite size, so the non-circular beam shape is apparent in the image. The peak/background ratio in this image is about 10. Given that the satellite image is many pixels in diameter, the integrated power/background ratio is much larger and this will improve position determinations. The background has some contribution from noise, but is also contaminated by many other bright satellites appearing outside the primary FOV of the antenna (not to mention calibration errors on CasA). This signal/background ratio can be improved by taking multiple images of the satellite at times spaced by fractions of an hour or more. The multi-image approach is limited since the satellite is expected to move no more than $\sim 10^\circ$ in a 24 hour day. Another approach is to image satellites outside the FOV and subtract them off (peeling). Further studies are required to see how signal/background may be improved or if this is even necessary.

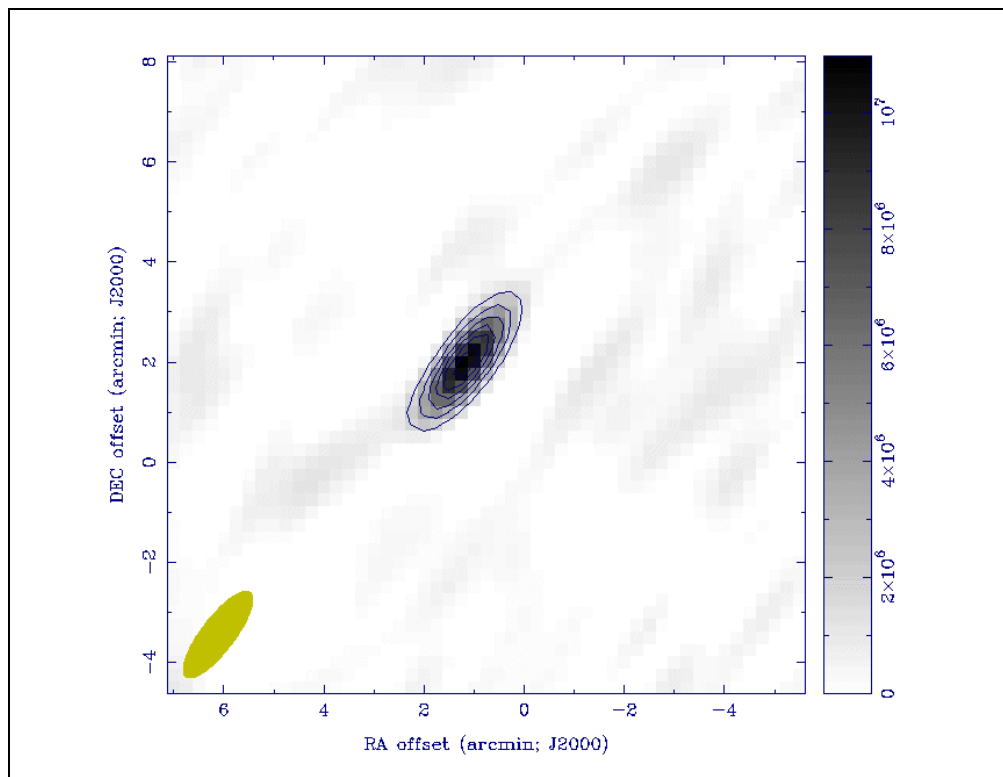


Figure 5: Blowup of a small region around one satellite. The resolution of the satellite image is limited by the natural beam width (point spread function) of the array. Even by eye it is obvious that the point-like satellite position can be determined to scales much smaller than the beam width.

As a final demonstration of technique for satellite position determination fig. 6 plots results of an automatic point-source determination algorithm (“clean”) for fig. 5. Clean is a program which takes an image like fig. 5, and “deconvolves” the synthetic beam shape from the image. For reasons related to mathematical convergence, the deconvolution is not done using ordinary methods, but with an inspired technique invented by Hogbom.ⁱⁱ Since then Clark, Schwab, and other authors have contributed to improvement and extension of clean.

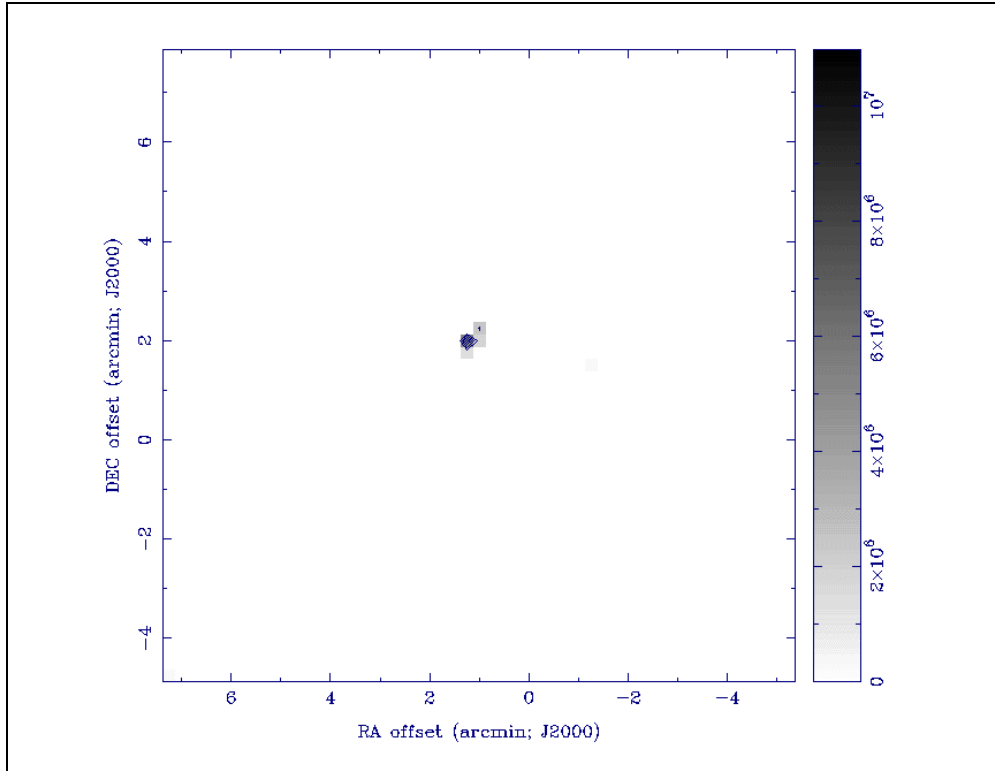


Figure 6: Starting with the a map centered on the region of fig. 5, we use clean to deconvolve the synthetic beam from the image. The clean components (identified point sources) are plotted here. This gives a graphical representation of how we automatically identify accurate satellite positions using data as in fig. 5.

The deconvolved image of the satellite is displayed in fig. 6. The intensity from the satellite is concentrated in a very small region, approximately 1 pixel. When maps are generated with a higher pixel density, the satellite power can be concentrated even more, giving a precise measure of the satellite position.

Notice that the deconvolved image has zero background level. This is a feature of the clean algorithm which strongly point sources over smooth background intensity. The broad/smooth background intensity of fig. 5 is not “seen” by the clean algorithm. For reference, note that there are variants of clean which do the opposite – enhancing and characterizing broad/smooth features while ignoring point sources. Since the satellites are known to be completely unresolved in these experiments, the point-source version of clean is the ideal tool for identifying satellites in the GEO belt.

Discussion

Our preliminary map of > 50 square degrees required about 4 hours observation time or 5 minutes per square degree at 4 GHz. The mapping speed varies inversely with frequency, so at 2 (8) GHz, the mapping speed would be 2.5 (10) minutes per square degree. This includes 3x overlapping of pointings to smooth sensitivity levels and substantial software overhead. With optimization, the observation times might be reduced by a factor a few.

Subarrays might improve satellite position throughput by ~20x on ATA350, but are not expected to be feasible with ATA42.

We have made no measurements of accuracy of satellite positions on this map, but we expect good performance. Recent studies of quasars at 1575 MHz shows definitively that we can determine their positions to an accuracy of ~3 arcsec. This accuracy will probably be met or even improved at 4 GHz because the images will have proportionally higher resolution. However, this accuracy is offset by the fact that currently, the ATA system temperature is ~2x higher at 4 GHz compared with 1.5 GHz. Longer calibrations and longer satellite tracks might make up the difference, though this will affect throughput.

Conclusions

This memo shows that ATA already has substantial infrastructure to map large areas of the GEO belt on useful time scales. Because it was the first time, the entire processing of this data required approximately 1-2 man weeks. Repeating the experiment would probably take less than half this time, and future automations can make the turnaround routine.

The greatest outstanding issue on this effort is to improve our calibration methods. The method used here is experimental, and already we have several ideas on improving it. We expect several iterations and perhaps different approaches will be necessary before we will obtain few-arcsec accuracy on satellites. Nonetheless, this first result is very encouraging!

¹ G. R. Harp, "[Customized Beam Forming at the ATA](http://ral.berkeley.edu/ata/memos/)," ATA Memo Series #51, available at <http://ral.berkeley.edu/ata/memos/>.

ⁱⁱ Hogbom, "Aperture Synthesis with a Non-Regular Distribution of Interferometer Baselines," (1974) Astronomy & Astrophysics Supplement Series 15, 417.